

Partial doubly differential cross sections for multiple ionization of argon, krypton, and xenon atoms by electron impact

M. A. Chaudhry,* A. J. Duncan, R. Hippler,† and H. Kleinpoppen

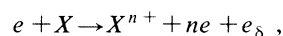
Atomic Physics Laboratory, Stirling University, Stirling FK9 4LA, Scotland, United Kingdom

(Received 30 June 1988)

Partial doubly differential cross sections for multiple ionization $d^2\sigma^{(n)}/dE d\Omega$ of argon, krypton, and xenon by electron impact have been measured as a function of incident electron energy and ejected electron energy, for argon up to Ar^{4+} , for krypton up to Kr^{5+} , and for xenon up to Xe^{8+} . Incident electron energies between 0.5 and 10 keV were used, while the electrons ejected at an angle of 90° to the incident electron direction were detected with energies between 20 and 270 eV. The doubly differential cross section (sum of partial doubly differential cross sections) for ionization for each gas has been compared with experimental data in the literature.

INTRODUCTION

Multiple ionization of atoms, as a result of photoionization^{1,2} and charged-particle impact,³ is of considerable interest because of its importance in the production of ion sources and in fields such as plasma physics, fusion physics, radiation physics, and astrophysics. Incident electrons, in particular, are known to produce multiple ionization of atoms via several processes such as direct multiple ionization,⁴ multiple ionization involving correlation⁵ between electrons, ionization of inner shells followed by Coster-Kronig⁶ and/or Auger⁷ transitions, and ionization followed by a core relaxation process⁸ (shake-off). In recent investigations of multiple ionization of rare-gas atoms by electron impact, total and partial ionization cross sections have been measured by Schram *et al.*,⁹ Nagy *et al.*,¹⁰ and Krishnakumar and Srivastava¹¹ for nonrelativistic electron energies, and Müller *et al.*¹² for relativistic electron energies. In addition, Opal *et al.*¹³ and Oda *et al.*¹⁴ have measured doubly differential cross sections for ionization of some gaseous atoms, while Van der Wiel and Wiebes¹⁵ have obtained differential cross sections for multiple ionization of rare-gas atoms by measuring the energy loss of the incident electrons in coincidence with the ions of different charge states. The only doubly differential cross-section data for multiple ionization available over a range of incident and ejected electron energies are for argon¹⁶ and for xenon¹⁷ atoms. Here we have investigated partial doubly differential cross sections for the collision reaction



where X is an atom of argon, krypton, or xenon, e_δ is the detected electron, and n is the charge state of the ion produced. Detection of the secondary electron e_δ in coincidence with the product X^{n+} enables a particular n -fold ionization process to be identified and studied. In this way, measurements have been made of partial doubly differential cross sections for n -fold ionization $d^2\sigma^{(n)}/dE d\Omega$ [or $(n+)$ DDCS] which are differential in the ejected electron energy E and solid angle Ω .

EXPERIMENTAL TECHNIQUE

Figure 1 shows schematically the experimental arrangement for measuring $(n+)$ DDCS by the electron-ion coincidence method. In this crossed-beam-type experiment, a beam of energetic electrons interacts with a dilute beam of atoms. A gun with a directly heated tungsten filament, capable of producing a high-energy focused beam of electrons having a diameter of about 2 mm in the interaction region, is mounted on a ceramic support and is allowed to float at high voltage while the voltage on the next electrode can be varied to focus the beam onto the last (collimating) electrode, which is kept at ground potential. A well-defined beam of atomic gas is obtained by effusing the gas through a nozzle consisting of a multicapillary array.¹⁸ Each capillary has a length of 3 mm and an internal diameter equal to 0.05 mm. A Faraday cup collects the electron beam after its interaction with the gas atoms and a Keithley electrometer monitors the electron current.

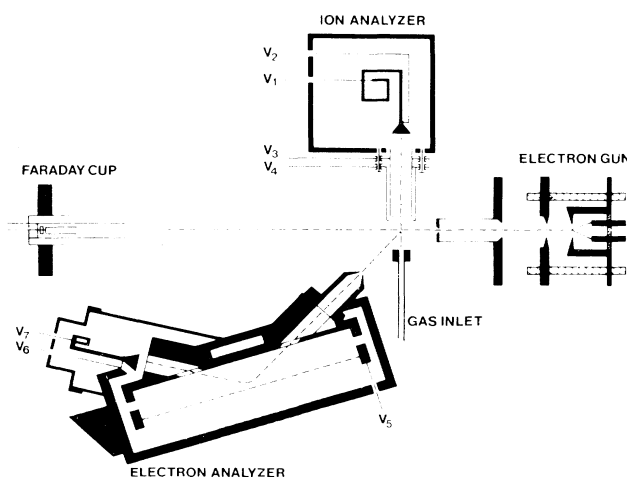


FIG. 1. Experimental setup for electron-ion coincidence experiments.

From the interaction region electrons ejected at 90° to the beam direction and in a narrow solid angle are accepted by a 30° parallel-plate electrostatic analyzer. Energy-analyzed electrons are detected by a channeltron. Electric potentials at the channeltron were varied so that the electrons incident at the channeltron always have an energy of 200 eV for maximum detection efficiency. Ions produced by the collision process are extracted by a small electric field between 15 and 25 V per centimeter and are directed into a time-of-flight (TOF) type analyzer. Inside the ion analyzer, ions are further accelerated by a potential difference of up to 100 V, depending upon the gas, and are allowed to drift in a field-free region of about 35 mm length. At the end of the drift tube the ions are accelerated by applying a negative potential of about 4 kV at the cone of the channeltron to ensure efficient detection¹⁹ of all ion species. The potential at the closed end of the channeltron was varied to keep the amplification of the channeltron constant throughout the experiment. The electric field for ion extraction was produced by applying equal and opposite potentials to the surfaces of the ion analyzer drift tube and the gas inlet nozzle adjacent to the interaction region which was therefore effectively at ground potential. As the entrance slit of the electron analyzer was also at ground potential the energy of the ejected electrons was unaffected. Also, since the entrance of the electron analyzer was close to the interaction region, the deviation in the path of the ejected electrons produced by the extraction field was negligible in the energy region used in these experiments.

The time delay between the arrival of the ejected electron and the product ion at the respective channeltrons gives information about the charge state of the ion and Figure 2 shows such a time spectrum for argon ions. Peaks for charge states $1+$ to $3+$ can be seen. From such a spectrum, after subtraction of random coincidences, the number of true coincidence events $N_c^{(n)}$ is related to the $(n +)$ DDCS by

$$\frac{d^2\sigma^{(n)}}{dE d\Omega} = \frac{N_c^{(n)}}{N_i} \frac{\sigma_i}{\Delta E \Delta\Omega \epsilon_\delta},$$

where σ_i is the total cross section for ion production, N_i the number of detected ions, ϵ_δ the efficiency of the detection system, and ΔE and $\Delta\Omega$ are respectively, the energy bandwidth and the solid angle associated with the electron analyzer. For σ_i the values of Schram, Boerboom, and Kistemaker⁹ have been used. The electron analyzer was operated with a modest resolution of 10% and had an acceptance angle of approximately 0.002 sr.

The doubly differential cross section $d^2\sigma/dE d\Omega$ (or DDCS) for ionization was found from the data for the partial doubly differential cross sections, $d^2\sigma^{(n)}/dE d\Omega$, using the relation

$$\frac{d^2\sigma}{dE d\Omega} = \sum_n \frac{d^2\sigma^{(n)}}{dE d\Omega}.$$

The results also made it possible to calculate the mean charge $\bar{n}(E)$ of the ions detected in coincidence with the secondary electrons of energy E , according to

$$\bar{n}(E) = \frac{\sum_n (N_c^{(n)} n)}{\sum_n N_c^{(n)}}.$$

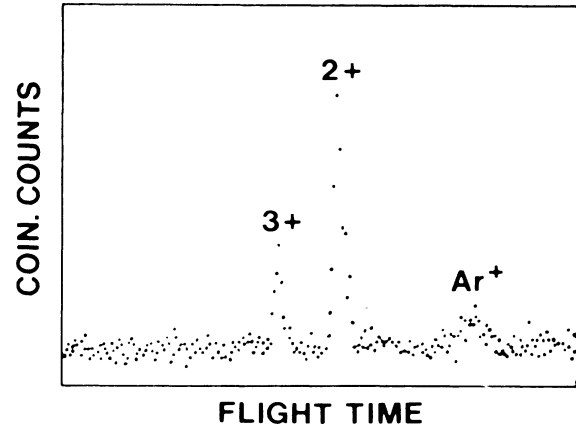


FIG. 2. Time-of-flight (TOF) spectrum of argon ions detected in coincidence with 200-eV secondary electrons, incident electron energy being 1.0 keV.

RESULTS AND DISCUSSION

Argon

Figure 3 shows the relative values of the DDCS plotted against secondary electron energy for incident electron energies of 1.0, 1.5, and 2.0 keV. Similar results obtained by Opal *et al.*,¹³ for 500-eV incident electron energy, are also shown for comparison. Electrons ejected from autoionization states have definite sharp energies and the corresponding spectrum is superimposed over the continuous part of the spectrum due to direct ionization

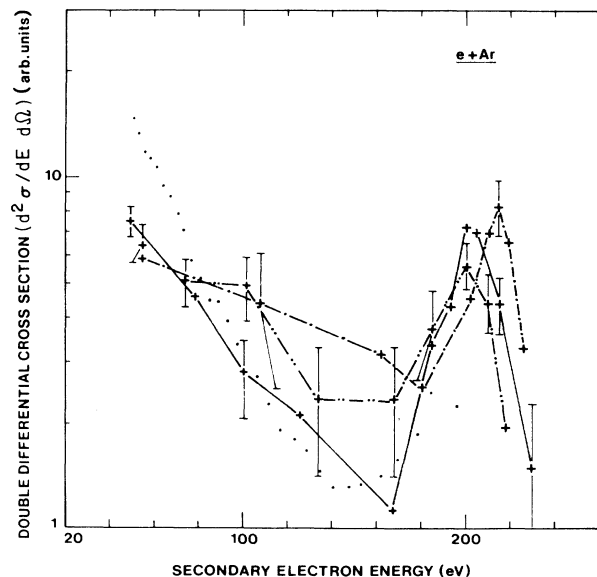


FIG. 3. Measured DDCS values drawn against secondary electron energy for incident electron energies of — — —, 2.0 keV; — · — · —, 1.5 keV; and · · · · ·, 1.0 keV. The similar results of Opal *et al.* for incident electron energy of 500 eV are shown as · · · · ·. The present results were normalized at 100 eV to the results of Opal *et al.* (Ref. 13). Lines are to guide the eye.

which, otherwise, generally exhibits^{13,14,20} a smooth decrease with increase in the energy of the emitted electrons. The higher values of the DDCS around 200 eV, secondary electron energy, are, in this case, due to the strong *LMM* Auger²¹ electron transitions. In general, the present results seem to agree with the results of Opal *et al.*¹³ in spite of the difference in incident electron energies.

Figures 4, 5, and 6(a) show relative values of the $(n+)$ DDCS and the DDCS plotted against secondary electron energy for incident electron energies of 1.0, 1.5, and 2.0 keV, respectively. In general, the $(1+)$ DDCS shows a rapid decrease¹⁶ with increase of secondary electron energy. It is also evident that the peaks in the $(3+)$ DDCS, which result from Auger transitions $L_{23}M_1M_{23}$, occur at a secondary electron energy which is 10–15 eV lower²² than the energy of the peaks in the $(2+)$ DDCS values which are due perhaps to the Auger transitions $L_{23}M_{23}M_{23}$. This observation also agrees with similar findings of Hippler *et al.*²³

Figure 6(b) shows the variation of mean charge $\bar{n}(E)$ with the secondary electron energy. It is evident that

low-energy secondary electrons are mostly associated with single ionization, while electrons around 200 eV, where $\bar{n}(E)$ has a value higher than 2, are mostly associated with multiply charged ions.

Figure 7 shows the $(n+)$ DDCS for $n=1-4$ plotted against the incident electron energy. The ejected electron energy was 200 eV. The values of the $(2+)$ DDCS are always higher than those of the $(1+)$ DDCS due to the strong *LMM* Auger transitions in this ejected electron energy region. Ions with higher charge states such as Ar^{3+} and Ar^{4+} result probably from vacancies in the L_1 subshell which decay via Coster-Kronig transitions²⁴ (93.4%) to L_{23} subshells followed by Auger electron emissions ($L_{23}MM$). The shakeoff process⁸ also contributes towards increasing the ionic charge as it has about a 15% probability of producing a vacancy in the outermost shell when there is an initial vacancy in the L shell. Another feature is an increase, most noticeable in the case of $(4+)$ DDCS, around 6-keV incident electron energy. This effect is probably due to the contribution of K -shell ionization which, followed by *KLL* and *LMM* Auger transitions, can result in additional multiple ionization.

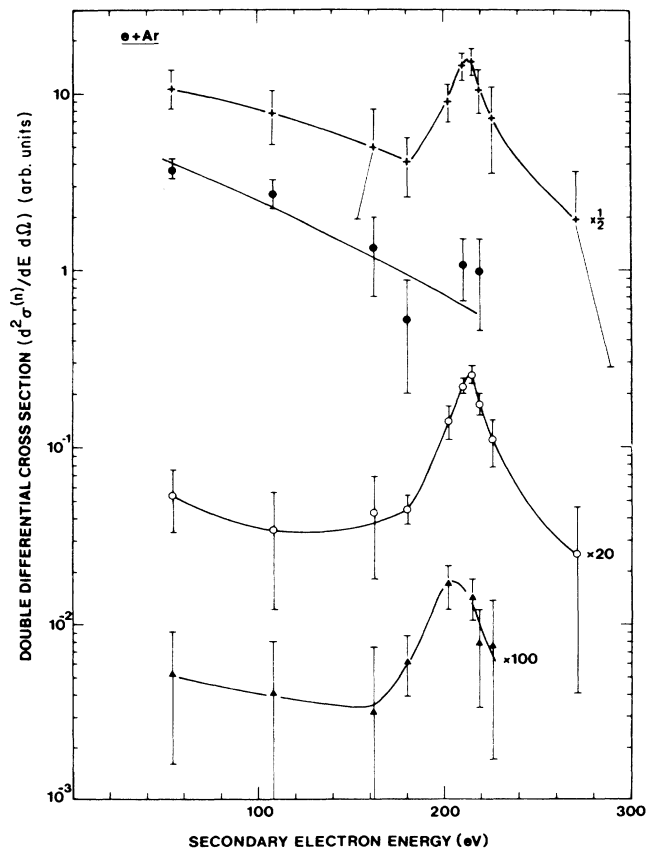


FIG. 4. Relative values of the $(n+)$ DDCS and the DDCS plotted against secondary electron energy, incident electron energy being 1.0 keV. Measurements are denoted \bullet , Ar^+ ; \circ , Ar^{2+} ; \blacktriangle , Ar^{3+} . The DDCS is marked +. The $(2+)$ DDCS, $(3+)$ DDCS, and DDCS have been divided by 20, 100, and $\frac{1}{2}$, respectively. Lines are to guide the eye.

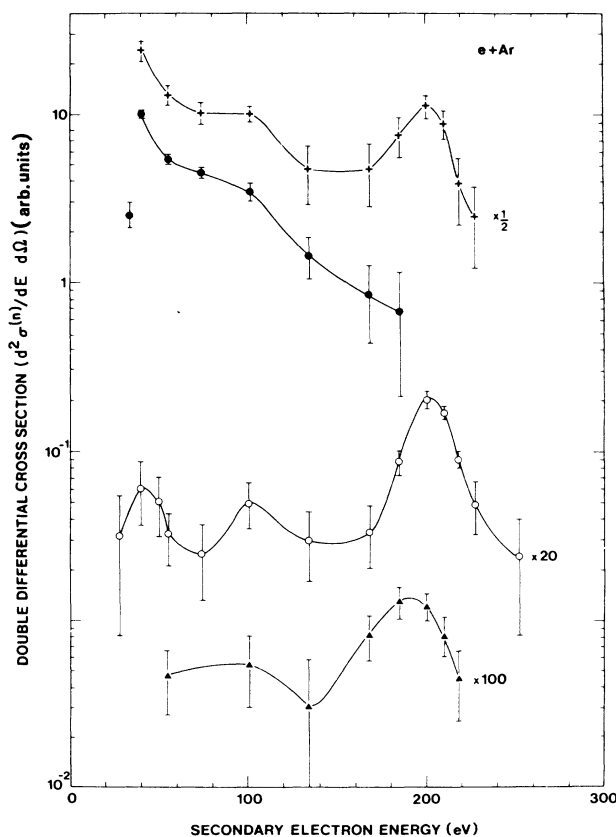


FIG. 5. Relative values of the $(n+)$ DDCS and the DDCS plotted against secondary electron energy, incident electron energy being 1.5 keV. Measurements are denoted by \bullet , Ar^+ ; \circ , Ar^{2+} ; and \blacktriangle , Ar^{3+} . The DDCS is marked +. The $(2+)$ DDCS, $(3+)$ DDCS, and DDCS have been divided by 20, 100, and $\frac{1}{2}$, respectively. Lines are to guide the eye.

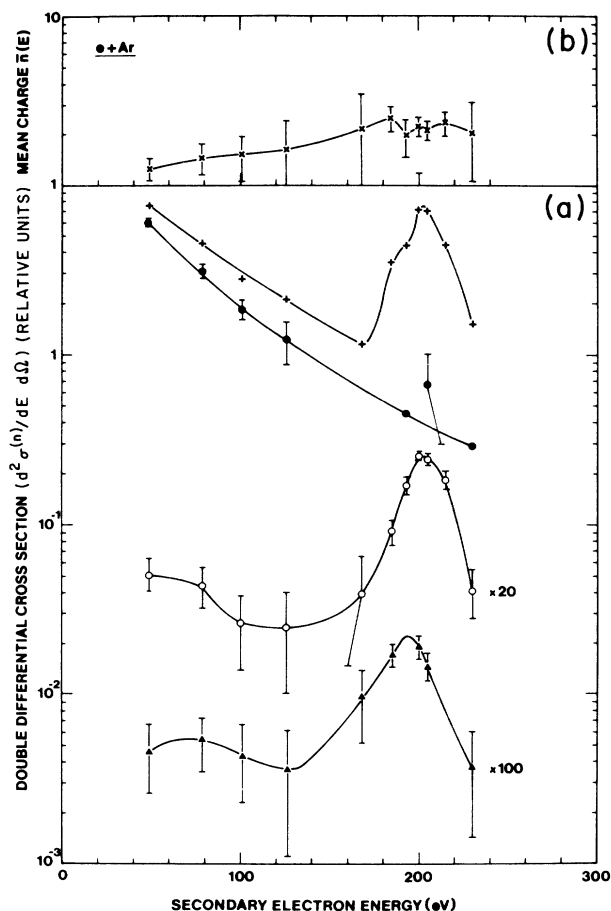


FIG. 6. (a) The $(n+)$ DDCS plotted against secondary electron energy, incident electron energy being 2.0 keV. Measurements are denoted by \bullet , Ar^+ ; \circ , Ar^{2+} ; and \blacktriangle , Ar^{3+} . The DDCS is marked $+$. The $(2+)$ DDCS and $(3+)$ DDCS have been divided by 20 and 100, respectively. Lines are to guide the eye. (b) Values of mean $\bar{n}(E)$ plotted against secondary electron energy. Lines are to guide the eye.

Krypton

Figure 8 shows a TOF spectrum for krypton ions detected in coincidence with secondary electrons of 85-eV energy, incident electron energy being 10.0 keV. Peaks for ions having charge states 1+ to 5+ can be seen. Krypton gas consists of a number of isotopes so that each peak is made up of several peaks,¹ one for each isotope. The inset in the figure shows the peak for Kr^{2+} more clearly with separate peaks for the various isotopes identified.

Figure 9 shows the relative values of the $(n+)$ DDCS and the DDCS plotted against secondary electron energy for an incident electron energy of 10.0 keV. The present measurements of the DDCS are found to display a secondary electron energy dependence similar to that found by Opal *et al.*¹³ Oda *et al.*¹⁴ obtained DDCS values which are clearly the result of superposition of a spectrum due to electrons emitted from autoionization transitions, such

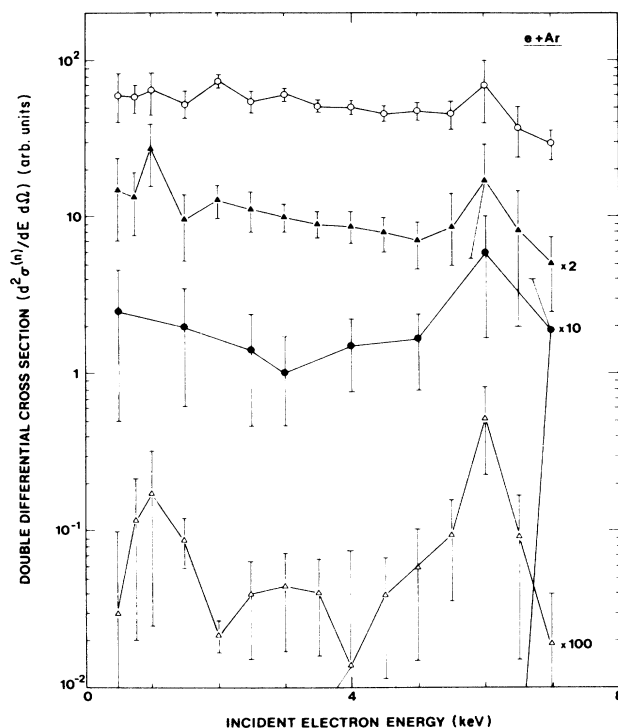


FIG. 7. The $(n+)$ DDCS plotted against incident electron energy for 200-eV secondary electron energy. Measurements are for \bullet , Ar^+ ; \circ , Ar^{2+} ; \blacktriangle , Ar^{3+} ; and \triangle , Ar^{4+} . The $(1+)$ DDCS, $(3+)$ DDCS, and $(4+)$ DDCS have been divided by 10, 2, and 100, respectively. Lines are to guide the eye.

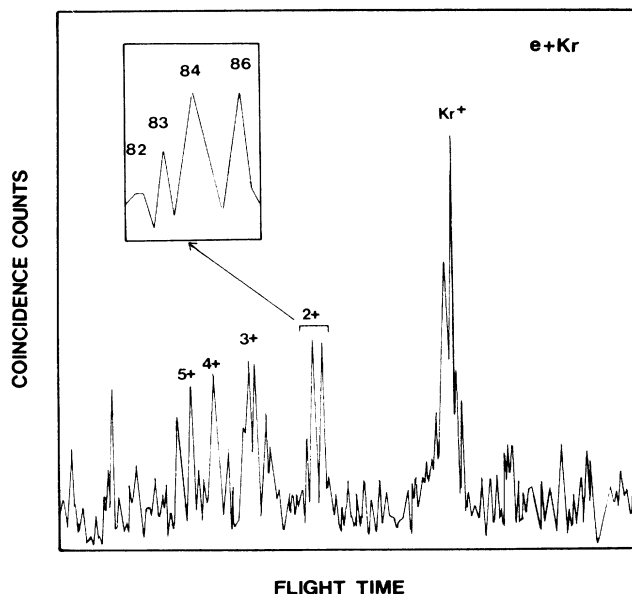


FIG. 8. Typical TOF spectrum for krypton ions formed as a result of electron impact on krypton atoms. The inset shows the isotopic spread of the peak for the Kr^{2+} ions.

as MNN , and a spectrum due to electrons ejected as a result of a process of direct ionization. Our DDCS values also exhibit maxima in the regions of the strong autoionization transitions.²¹

The $(n+)$ DDCS values in general, and the $(1+)$ DDCS in particular, show a rapid decrease with increase of ejected electron energy. The following additional features can also be noted concerning the behavior of $(n+)$ DDCS values.

(i) The $(2+)$ DDCS shows a broad maximum in the re-

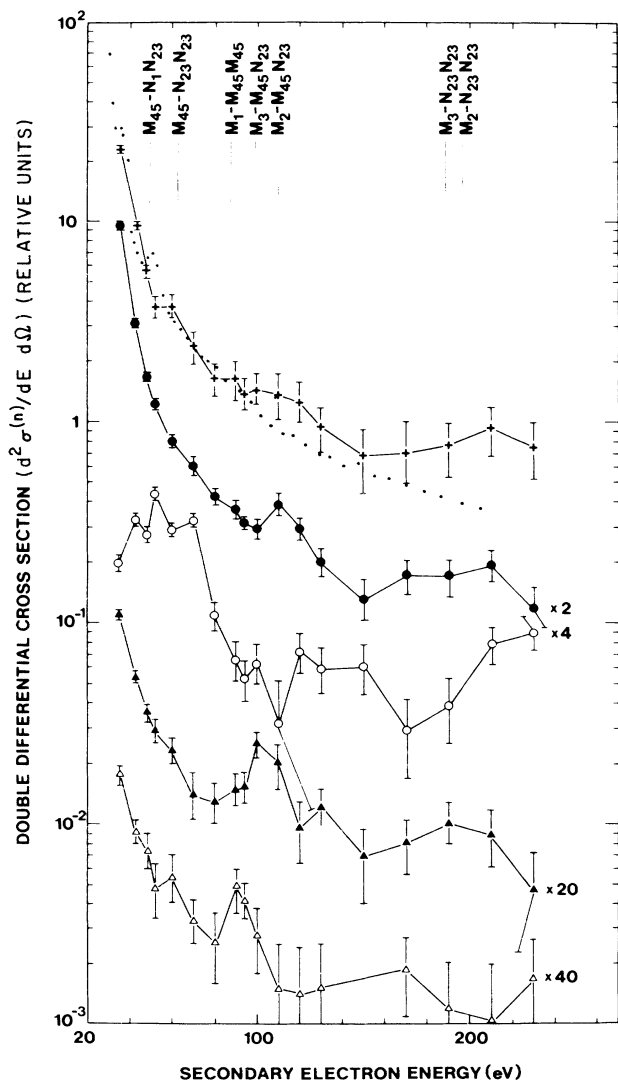


FIG. 9. Relative values of the $(n+)$ DDCS plotted against secondary electron energy, the incident electron energy being 10.0 keV. Measurements are for \bullet , Kr^+ ; \circ , Kr^{2+} ; \blacktriangle , Kr^{3+} ; and \triangle , Kr^{4+} . The DDCS values are marked +. The experimental results of Opal *et al.* (Ref. 13) are shown as $\cdot \cdot \cdot$. The present values of the DDCS were normalized to the data of Opal *et al.* (Ref. 13) at 85-eV secondary electron energy. The $(1+)$ DDCS, $(2+)$ DDCS, $(3+)$ DDCS, and $(4+)$ DDCS have been divided by 2, 4, 20, and 40, respectively. Lines are to guide the eye.

gion of the strong MNN Auger transitions around 40–60 eV. The increase of the values of the $(2+)$ DDCS beyond 170-eV secondary electron energy is also due perhaps to MNN Auger transitions²⁵ in this region.

(ii) The $(3+)$ DDCS shows a rapid decrease with increase of secondary electron energy except for a broad peak at about 100-eV secondary electron energy. This

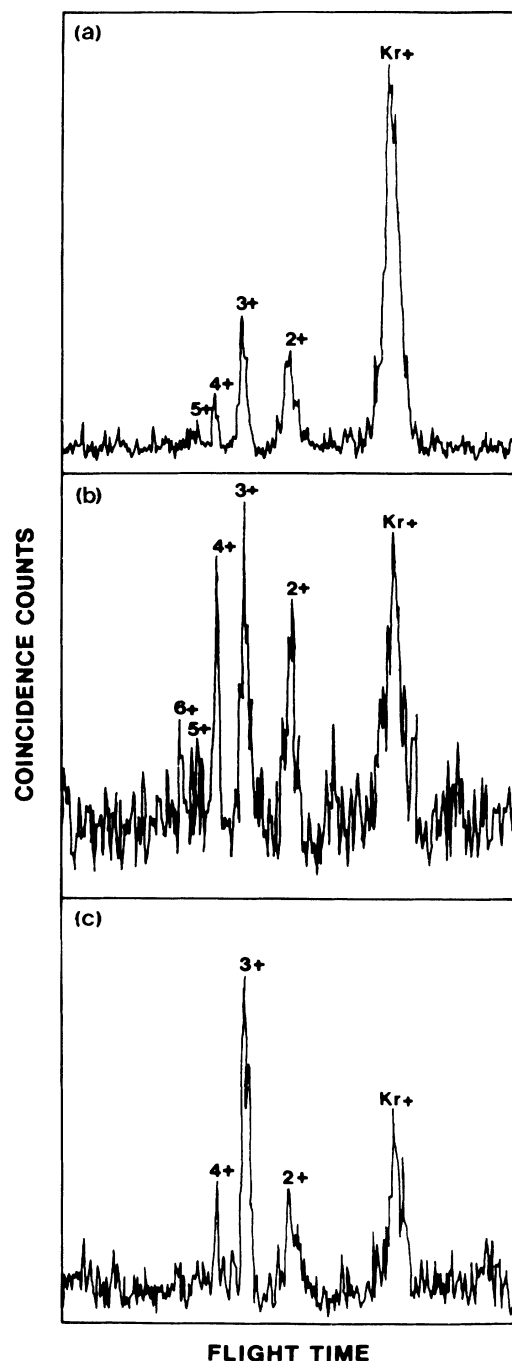


FIG. 10. TOF spectra for krypton ions detected in coincidence with secondary spectra for krypton ions of (a) 15 eV; (b) 63.5 eV; (c) 70.0 eV. The incident electron energy was 10.0 keV.

peak probably results from the decay of vacancies in the M_{23} subshells by Coster-Kronig transitions such as $M_{23}M_{45}N_{23}$ followed by Auger electron emissions such as $M_{45}N_{23}N_{23}$.

(iii) The $(4+)$ DDCCS also shows a peak at about 90-eV secondary electron energy. This peak could be due to a vacancy in the M_1 subshell decaying by the highly probable²⁶ Coster-Kronig transition, $M_1M_{45}M_{45}$, followed by simultaneous emission of two similar Auger electrons such as $M_{45}N_{23}N_{23}$, thus giving rise to four vacancies in the outermost shell.

Figure 10 demonstrates the relative abundances of krypton ions of various charge states when these are detected in coincidence with secondary electrons of different energies. It can be seen that low-energy secondary electrons are predominantly associated with Kr^+ ions. With an increase in secondary electron energy, the Kr^+ ions show a rapid decrease, while ions of a higher charge state are more abundant when the secondary electron energies are in the regions of autoionization transitions.

Figure 11 shows relative values of the $(n+)$ DDCCS plotted against incident electron energy, secondary electron energy being 60 eV. Apart from showing a slight overall decrease in the values, as dictated by the total ionization cross-section⁹ data for this incident electron energy region, the values of the $(n+)$ DDCCS show small changes at the L -subshell ionization potentials.

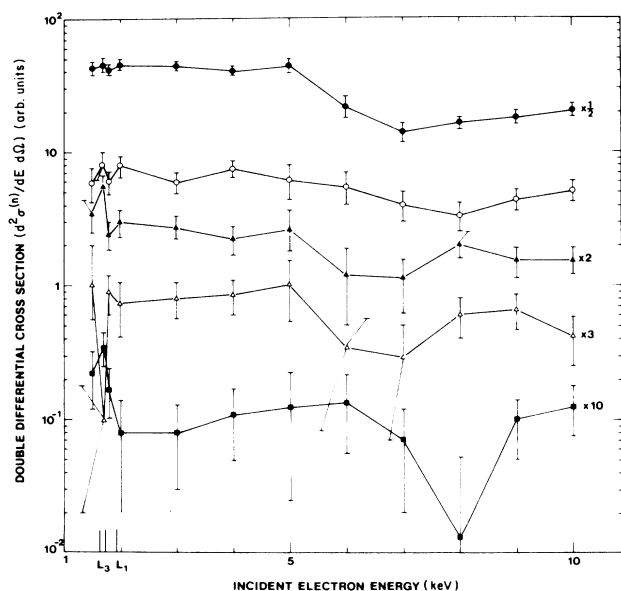


FIG. 11. The $(n+)$ DDCCS plotted against secondary electron energy, incident electron energy being 10.0 keV. Measurements are for \bullet , Kr^+ ; \circ , Kr^{2+} ; \blacktriangle , Kr^{3+} ; \triangle , Kr^{4+} ; and \blacksquare , Kr^{5+} . The $(1+)$ DDCCS, $(3+)$ DDCCS, $(4+)$ DDCCS, and $(5+)$ DDCCS have been divided by $\frac{1}{2}$, 2, 3, and 10, respectively. Lines are to guide the eye.

Xenon

A TOF spectrum of xenon ions detected in coincidence with ejected electrons of different energies for an incident electron energy of 6.0 keV has been shown in Ref. 17, where some measurements for the $(n+)$ DDCCS for $n=1-3$ and the DDCCS have been given as a function of the ejected electron energy. These results have now been extended to include the $(n+)$ DDCCS data for $n=4-6$, and Fig. 12 shows these extended measurements. The features noticeable in the $(n+)$ DDCCS are as follows.

(i) A rapid decrease up to about 80-eV secondary electron energy, after which the decrease becomes less rapid and in some cases, such as the $(3+)$ DDCCS, there does not seem to be any decrease up to about 300-eV secondary electron energy.

(ii) The $(2+)$ DDCCS, $(6+)$ DDCCS, and DDCCS show broad peaks at 30-eV secondary electron energy, due probably to the strong MNN Auger transitions in this region.

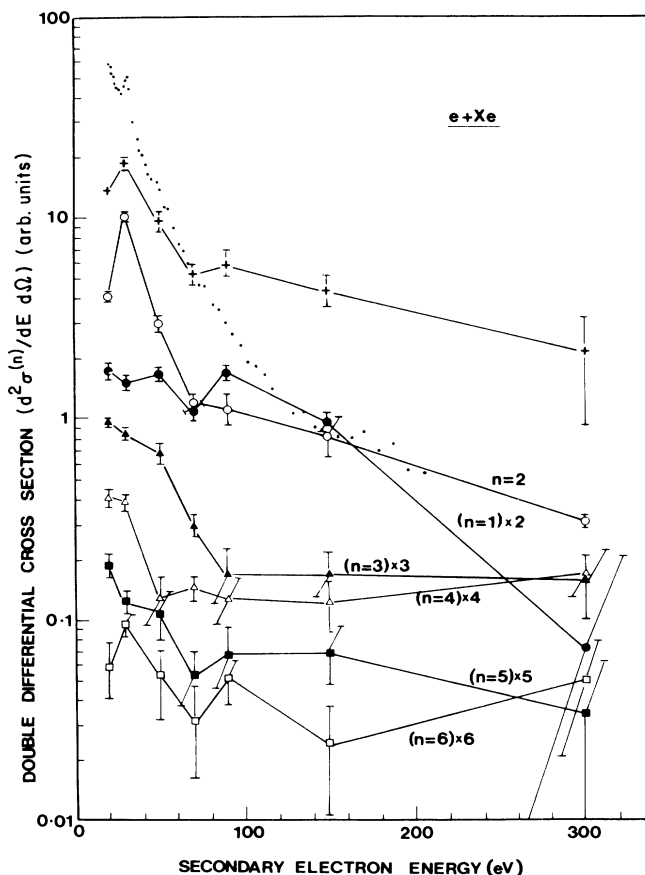


FIG. 12. Relative values of $(n+)$ DDCCS for \bullet , Xe^+ ; \circ , Xe^{2+} ; \blacktriangle , Xe^{3+} ; \triangle , Xe^{4+} ; \blacksquare , Xe^{5+} ; and \square , Xe^{6+} plotted against ejected electron energy. The incident electron energy was 6.0 keV. The DDCCS values are marked +. . . . shows the results of Opal *et al.* (Ref. 13). The $(1+)$ DDCCS, $(3+)$ DDCCS, $(4+)$ DDCCS, $(5+)$ DDCCS, and $(6+)$ DDCCS have been divided by 2, 3, 4, 5, and 6, respectively, for better presentation. Lines are to guide the eye.

Figure 12 also shows that our results for the DDCS agree generally with similar results of Opal *et al.*¹³ for 500-eV incident electron energy. However, at secondary electron energies greater than 100 eV our values for the DDCS are higher than those of Opal *et al.*¹³ This increase could be due to the several additional single²¹ and double²⁶ Auger transitions which are possible at 6.0-keV incident electron energy.

Conclusion

The first Born approximation can satisfactorily explain single ionization at impact velocities high compared to the orbiting electron velocity, but even in this case the processes involved in multiple ionization are not clear.³ At lower impact velocities, however, the ionization pro-

cesses become even more complicated due to the interactions between the projectile, the target nucleus, and the ejected electrons, and also because of the changes in the binding energies of the target electrons due to the presence of the charged projectile.²⁷ To find appropriate approximations for the solution of the many-body problem is a challenging goal for a theoretical physicist. Accurate data are, therefore, required not only for total and partial ionization cross sections but also for differential ionization cross sections, since the latter provide more critical tests for the theoretical calculations. The present data for partial doubly differential cross sections for argon, krypton, and xenon, will therefore be useful in extending our understanding of the phenomenon of multiple ionization and will provide a stringent test for any future theoretical model for the process.

*On leave from High Tension and Nuclear Research Laboratory, Government College, Lahore, Pakistan.

†Permanent address: Fakultät für Physik, Universität Bielefeld, D4800 Bielefeld, West Germany.

¹R. T. Short, C.-S. O, J. C. Levin, I. A. Sellin, L. Liljiby, S. Huldt, S.-E. Johansson, E. Nilsson, and D. A. Church, *Phys. Rev. Lett.* **56**, 2614 (1986).

²G. Mainfray, *J. Phys. (Paris) Colloq.* **46**, 113 (1985); T. S. Luk, H. Plummer, K. Boyer, M. Shahidi, H. Eggar and C. K. Rhodes, *Phys. Rev. Lett.* **51**, 110 (1983).

³L. H. Andersen, P. Hvelplund, H. Knudsen, S. P. Moller, A. H. Sorensen, K. Elsener, K. G. Rensfelt, and E. Uggerhoj, *Phys. Rev. A* **36**, 3612 (1987).

⁴F. D. Daniel, *Nucl. Instrum. Methods* **214**, 57 (1983); A. Kumar and B. N. Roy, *Can. J. Phys.* **56**, 1255 (1978).

⁵V. Schmidt, N. Sandner, H. Kuntzemüller, P. Dhez, F. Wiuleumier, and E. Kallne, *Phys. Rev. A* **13**, 1748 (1976).

⁶W. Mehlhorn, *Z. Phys.* **208**, 1 (1967).

⁷W. Mehlhorn, *Lectures on The Auger Effect* (University of Nebraska, Lincoln, 1969), and references therein.

⁸T. A. Carlson and C. W. Nester, Jr., *Phys. Rev. A* **8**, 2887 (1973).

⁹B. L. Schram, A. J. H. Boerboom, and J. Kistemaker, *Physica (Utrecht)* **32**, 185 (1966); B. L. Schram, *ibid.*, **32**, 197 (1966).

¹⁰P. Nagy, A. Skutlartz, and V. Schmidt, *J. Phys. B* **13**, 1249 (1980).

¹¹E. Krishnakumar and S. K. Srivastava, *J. Phys. B* **21**, 1055 (1988).

¹²A. Müller, W. Groh, U. Kneissl, R. Heil, H. Ströher, and E. Salzborn, *J. Phys. B* **16**, 2039 (1983).

¹³C. B. Opal, E. C. Beaty, and W. K. Peterson, *At. Data* **4**, 209 (1972).

¹⁴N. Oda, F. Nishimura, and S. Tahira, *J. Phys. Soc. Jpn.* **33**, 462 (1972).

¹⁵M. J. Van der Wiel and G. Wiebes, *Physica* **54**, 411 (1971), and references therein.

¹⁶R. Hippler, K. Saeed, A. J. Duncan, and H. Kleinpoppen, *Phys. Rev. A* **30**, 3328 (1984).

¹⁷M. A. Chaudhry, A. J. Duncan, R. Hippler, and H. Kleinpoppen, *Phys. Rev. Lett.* **59**, 2036 (1987).

¹⁸C. B. Lucas, *J. Phys. E* **6**, 991 (1973).

¹⁹J. P. Ravon, *Nucl. Instrum. Methods* **211**, 7 (1982).

²⁰G. N. Ogurtsov, *Zh. Eksp. Teor. Fiz.* **64**, 1149 (1973) [*Sov. Phys. — JETP* **37**, 584 (1973)].

²¹W. A. Coglan and R. E. Clausing, *At. Data* **5**, 317 (1973).

²²R. F. Mathis and D. A. Vroom, *J. Chem. Phys.* **64**, 1146 (1976).

²³R. Hippler, J. Bossler, and H. O. Lutz, *J. Phys. B* **17**, 2453 (1984).

²⁴M. O. Krause, *J. Phys. Chem. Ref. Data* **8**, 307 (1979).

²⁵W. Mehlhorn, *Z. Phys.* **187**, 21 (1965).

²⁶W. Mehlhorn, in *Auger-Electron Spectroscopy of Core Levels of Atoms in Atomic Inner-shell Physics*, edited by B. Craseman (Plenum, New York, 1985), p. 121.

²⁷W. Brandt and G. Basbas, *Phys. Rev. A* **27**, 578 (1983).